Title

A theoretical and experimental study of high resolution EEG based on surface Laplacians and cortical imaging

Journal

Clinical Neurophysiology, 90(1)

ISSN

1388-2457

Authors

Nunez, PL
Silberstein, RB
Cadusch, PJ
et al.

Publication Date

1994

DOI

10.1016/0013-4694(94)90112-0

Electroencephalography and clinical Neurophysiology, 90 (1994) 40–57

EEG 92124

A theoretical and experimental study of high resolution EEG based on surface Laplacians and cortical imaging

P.L Nunez [a,*], R.B. Silberstein [b], P.J. Cadusch [b], R.S. Wijesinghe [a], A.F. Westdorp [a] and R. Srinivasan [a]

[a] *Brain Physics Group, Dept. of Biomedical Engineering, Tulane University, New Orleans, LA (USA), and*
[b] *Swinburne Centre for Applied Neurosciences, Swinburne University of Technology, Melbourne (Australia)*

(Accepted for publication: 27 August 1993)

Summary Two different methods to improve the spatial resolution of EEG are discussed: the surface Laplacian (e.g., current source density) and cortical imaging (e.g., spatial deconvolution). The former methods tend to be independent of head volume conductor model, whereas the latter methods are more model-dependent. Computer simulations of scalp potentials due to either a few isolated sources or 4200 distributed cortical sources and studies of actual EEG data both indicate that the two methods provide similar estimates of cortical potential distribution. Typical correlation coefficients between either spline-Laplacian or cortical image and simulated (calculated) cortical potential are in the 0.8–0.95 range, depending partly on CSF thickness. By contrast, correlation coefficients between simulated scalp and cortical potential are in the 0.4–0.5 range, suggesting that high resolution methods provide much better estimates of cortical potential than is obtained with conventional EEG. The two methods are also applied to steady-state visually evoked potentials and spontaneous EEG. Correlation coefficients obtained from real EEG data are in the same general ranges as correlations obtained from simulations. The new high resolution methods can provide a dramatic increase in the information content of EEG and appear to have widespread application in both clinical and cognitive studies.

Key words: EEG; High resolution; Spatial resolution; Surface Laplacian; Cortical imaging; Current source density; Spatial deconvolution

Limitations of conventional EEG

Electroencephalography enjoys a distinct advantage over other brain imaging methods because of its high temporal resolution, which allows for direct studies of brain dynamic function at millisecond time scales. However, the severe limitations of the spatial resolution of conventional EEG have limited the available information to a substantial degree. In practice, poor spatial resolution in conventional EEG is due to the following factors.

(1) Limited spatial sampling. The use of about 20 electrodes over the entire scalp in the standard 10/20 system results in a center-to-center average electrode spacing of about 6 cm. The addition of more electrodes may not add significantly to the information content of an EEG record unless additional steps are taken. This limitation occurs because of factors 2 and 3, discussed below.

(2) Spatial smearing and other distortions by the head volume conductor. Part of EEG folklore in recent years has been the following idea: If a "recording electrode" is placed on the scalp and potentials are recorded with respect to a "quiet reference," the recorded potential is mainly due to "generators" close to the electrode. This idea is generally inaccurate as illustrated by theoretical considerations of sources in concentric sphere models (Nunez 1981, 1986).

An illustration of the limitations of unprocessed scalp potential maps is shown in Fig. 1. In this example, 4200 sources at the macrocolumn scale are distributed over the inner hemisphere in the 3-sphere theoretical model. Scalp potential is assumed to be sampled at 48, 64, or 118 surface locations, approximately uniformly spaced over the scalp. Even with 118 sample locations (or 640, not shown), the surface potential map does not represent small or even moderate scale features of the source distribution. For example, patches of coherent activity of sizes smaller than about 5 cm are generally not revealed, even when electrode spacing is less than 1 cm.

(3) The reference electrode. The problems of unprocessed potential maps discussed above occur even in

* Corresponding author.

SSDI 0013-4694(93)E0214-Q

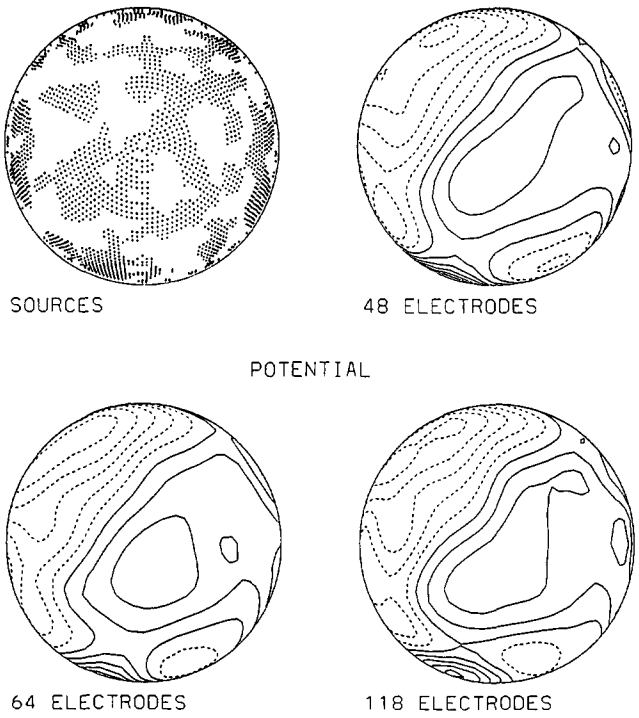

Fig. 1. Upper left: radial dipole sources at the macrocolumn scale (~ 3 mm) are simulated. There are a total of 4200 sources distributed non-uniformly over the "cortex." Source magnitudes are given in terms of the potential difference across the cortex, which are here assumed to vary between ± 200 μV consistent with micro-EEG electrode studies of spontaneous EEG (Lopes da Silva et al. 1978; Petsche et al. 1984; review by Nunez 1990b). Filled spaces indicate positive sources, empty spaces negative sources. The 3 other figures show estimated scalp potential based on discrete sampling at 48, 64 or 118 scalp locations. Each of the 4200 sources contributes to each of these "electrode" positions, as predicted by the 3-concentric sphere model of the head. Even in the limit of very high spatial sampling (e.g., 640 "electrodes," not shown), the scalp potential map fails to show small or moderate scale source features, even in the case of no reference electrode contamination. The maximum magnitude of predicted scalp potential in this example is about 11 μV, but depends critically on the sizes of the source clumps. All plots on spherical surfaces shown in this paper were constructed using NCAR (National Center for Atmospheric Research) graphics, developed to map isocontours of pressure, temperature, etc. on the earth's surface. The contours wrap around the sphere and appear compressed at the edge of the plots. Regions near the edge can be viewed by rotating the sphere.

the idealized case of potentials recorded with respect to infinity. However, such idealized references are generally not available in EEG practice. We have discussed reference electrode issues in detail in earlier studies (Nunez 1981, 1988, 1990a; Nunez et al. 1991), which reinforce the widely held notion that reference-free methods (e.g., the surface Laplacian or close bipolar recordings) offer significant advantages in many if not most applications.

The problem of interpretation of scalp potentials in terms of the underlying sources is further illustrated in Fig. 2. In both of these examples, a right ear reference is assumed. The blank space adjacent to the right ear indicates that no sources are located within about 5 cm of the ear (e.g., a "quiet" reference). The source distribution on the left consists of 3 major clumps of sources indicated by the + and − signs, within a background of random positive and negative sources (blank spaces denote negative sources at every location except the right ear region). These 3 major source clumps are unchanged in the simulation at the right; however, background sources in the right side plot also form clumps. Comparison of the two potential plots shows that the potential directly above the positive clump switches from positive to negative and the potential above the lower negative clump switches from negative to positive even though the 3 underlying source clumps are unchanged. These simulations illustrate limitations of conventional EEG due to the non-local character of scalp potentials, even when no sources are located close to the reference electrode.

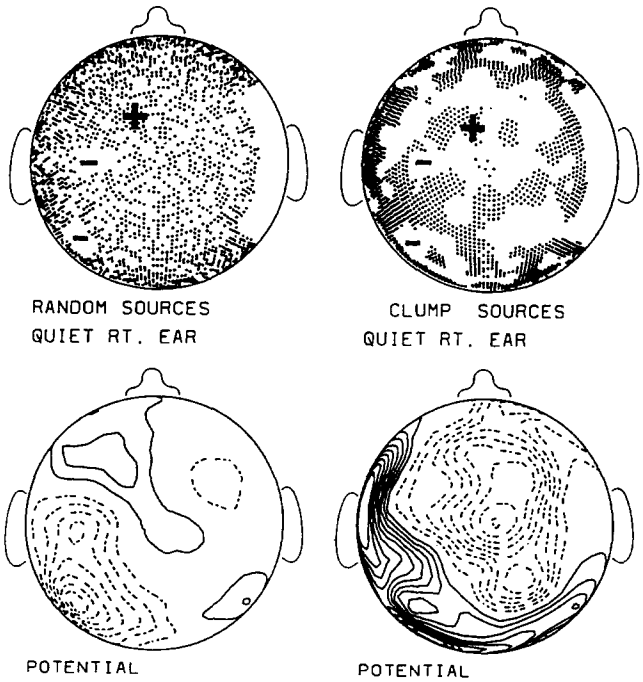

Fig. 2. Simulations with radial dipole sources at the macrocolumn scale. Dots indicate positive source magnitudes. Empty spaces are negative magnitudes except near the right ear where no sources occur. The 3 clumped regions denoted by plus and minus signs do not change. However, background sources change from random to clumped (upper right). The corresponding scalp potential maps (with respect to right ear reference) are calculated using the 3-concentric sphere model of the head. The scalp potential just above the positive clump changes from positive to negative, and the scalp potential above the lower negative clump changes from negative to positive, even though the underlying source clumps are unchanged. Again, this simulation illustrates the non-local character of raw scalp potentials, even with a "quiet" reference.

High resolution EEG

We define EEG spatial resolution as the minimum size of a spatial pattern of cortical sources which can be distinguished from other like patterns using scalp recordings. With this definition, the spatial resolution of conventional EEG is typically no better than 5 cm and can be much worse, depending partly on reference electrode effects. Two general methods have been proposed to improve the spatial resolution of scalp recorded potentials: the surface Laplacian (i.e., current source density) and cortical imaging (i.e., spatial deconvolution).

(1) The surface Laplacian

These methods provide estimates of local current density flowing perpendicular to the skull into the scalp. Cortical surface potential can also be estimated from the surface Laplacian if desired. Estimation of source nature or location (e.g., radial/tangential, cortical/non-cortical) may be obtained as a separate step based on knowledge of the underlying physiology and anatomy. However, since the Laplacian is much more sensitive to local sources (both tangentially and in depth), most significant contributions to Laplacian maps are believed to be due to cortical sources.

Actually, there are many versions of the Laplacian estimate (Nunez 1989a, 1990a,b), ranging from the use of groups of five or more local electrodes (Hjorth 1975; Katznelson 1981a; Nunez 1981; Gevins 1989; Gevins et al. 1990; Nunez and Pilgreen 1991) to global measures based on spline fits to recorded potentials (Perrin et al. 1987a,b, 1989; Nunez 1988, 1989a, 1990b; Gevins et al. 1991; Law 1991; Nunez et al. 1991; Law et al. 1993). The later (spline) methods act to bandpass data, with spatial filter characteristics chosen to match head volume conductor properties as closely as possible. The spline-Laplacian and spline-potential maps due to 5 isolated cortical sources are shown in Fig. 3. The Laplacian is much better at picking out details of the source distribution, although still limited to sources separated by about 3 cm in the case of 64 spatial samples (i.e., electrodes). Interpretation of the potential map may be further confounded by deep sources and/or reference electrode effects, neither of which have much effect on the Laplacian.

All Laplacian methods are reference independent. Furthermore, preliminary studies indicate that the spline-Laplacian tends to eliminate artifact caused by a single bad electrode (simulated by setting one potential to zero) or artifact generated outside the electrode array (e.g., eye movements). Spline-Laplacian estimates of the distributed cortical source distribution of Fig. 1 are shown in Fig. 4, based on the same sets of electrode arrays. By contrast to the potential map of Fig. 1, the Laplacian map of Fig. 4 converges to the actual

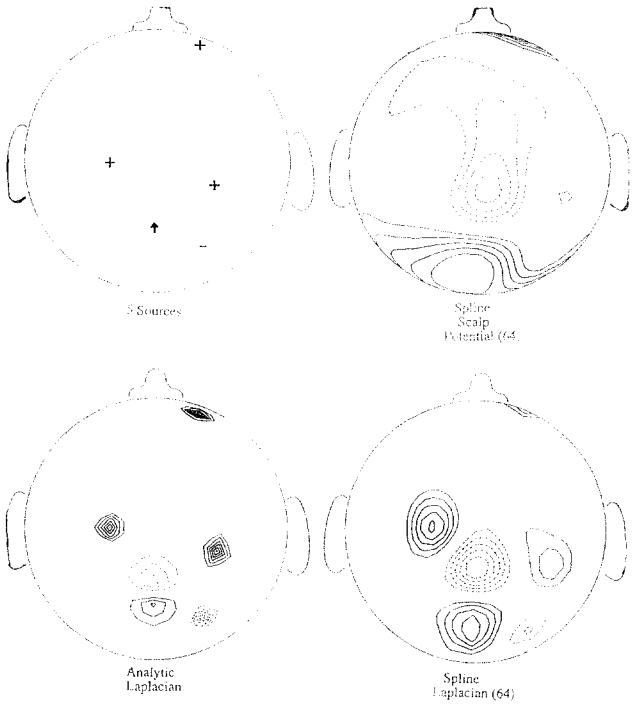

Fig. 3. Upper left: simulations involving 5 isolated neocortical sources: 1 tangential dipole (arrow) and 4 radial sources (+ or −). The 4 radial dipoles all have the same strength and depth. The single tangential dipole is located 0.5 cm deeper (e.g., in a sulcus) and has a strength 4 times larger (e.g., due to sources distributed in the depth of a sulcus). Upper right: the scalp potential distribution calculated using the 5 sources in the 3-concentric sphere model is sampled at 64 locations (e.g., electrodes) and fitted to the New Orleans 3-dimensional spline interpolation. This spline-potential distribution based on 64 samples is nearly identical to the exact (analytic) plot based on 660 surface points (not shown). In other words, no amount of sampling density is sufficient to pick out details of the source distribution. Lower left: the exact (analytic) surface Laplacian. Lower right: the surface Laplacian based only on the 64 discrete samples of potential, as obtained with the New Orleans spline algorithm.

source distribution as electrode density is increased. Also, the addition of 20% random (e.g., spatially uncorrelated) noise to the potential map of Fig. 1 has minimal effect on the Laplacian of Fig. 4, due to the global spatial filtering properties of the spline-Laplacian.

(2) Cortical imaging

These methods make use of a volume conductor model of the head (usually a 3- or 4-concentric sphere model) to predict cortical surface potential from scalp potential (Nunez 1987a; Gevins 1990; Kearfott et al. 1991; Sidman 1991). In theory, more accurate estimates of cortical potential can be obtained using finite element models. For example, Yan et al. (1991) compared the accuracy of forward solutions obtained with a finite element model with those obtained in a layered sphere. In these simulations, differences between scalp potentials calculated with concentric spheres versus realisti-

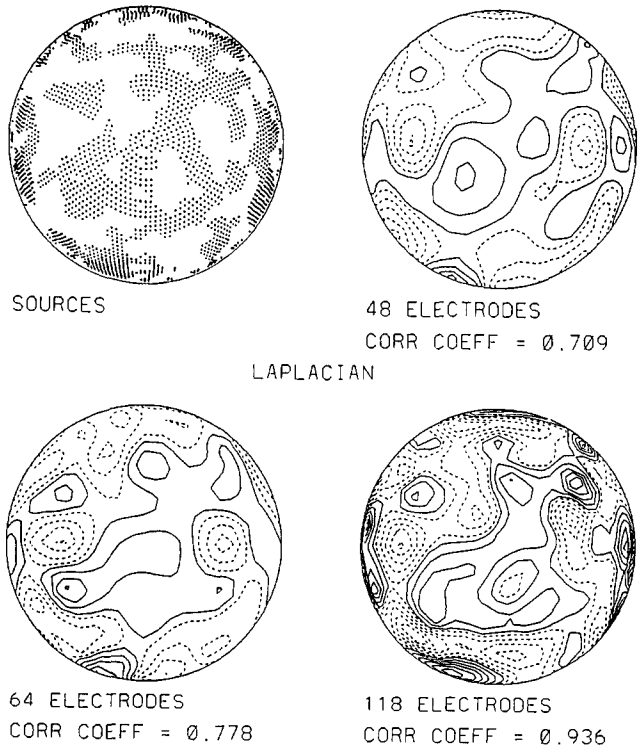

Fig. 4. Upper left: the same source distribution as shown in Fig. 1. Potentials are again sampled at 48, 64 or 118 scalp locations. These potentials are submitted to the spline-Laplacian algorithm which obtains estimates of appropriately smoothed Laplacian maps, based on a conservative view of uncertainty of volume conductor properties of the head. Correlation coefficients refer to a comparison between estimated and actual (analytic) Laplacian. The actual Laplacian shown in the upper right corner of Fig. 8 is very close to both the source distribution and Laplacian estimated with 118 "electrodes." The addition of 20% random (e.g., spatially uncorrelated) noise, sources of moderate magnitude (e.g., 30 μV) outside the array (e.g., eye movements), or 1 out of 64 samples set to zero potential (e.g., "bad electrodes") have minimal effects on the Laplacian maps estimated with 64 or 118 electrodes, due to the global smoothing properties of the spline.

cally shaped heads were typically in the 10–20% range. However, our limited knowledge of tissue boundaries and resistivities still results in significant uncertainty in the accuracy of these methods.

A recent contribution to EEG cortical imaging methods is the development of explicit criteria for choosing the optimum trade-off between smoothness and error for a given signal (Cadusch et al. 1992). This approach involves the use of a smoothing function. When smoothing is large, predicted cortical potential is similar to measured scalp potential. As smoothing is decreased, more and more detail is evident in the predicted cortical potential. However, at some intermediate value of the smoothing parameter, this detail becomes unreliable because of errors in the head model and/or noise in the signal. Thus, an optimum smoothing parameter may be chosen based on estimated uncertainty in the head model and signal-to-noise ratio of the signal. In summary, one tries to display just the right amount of detail in the spatial structure of the estimated cortical potential map.

With either Laplacian or cortical imaging methods an additional prediction of cortical source density can be obtained; however, this step requires critical assumptions about the location (e.g., in the cortex) and nature (e.g., mix of radial and tangential dipoles) of the sources. Such assumptions must be based on additional physiological and anatomical information which may be much less reliable than estimates of cortical surface potential. Thus, we consider such source estimates as separate from the high resolution methods, which are then independent of any assumptions about the nature and location of sources. High resolution methods are viewed here as simply estimates of cortical surface potential and/or perpendicular skull current distribution.

An important advantage of Laplacian methods is their reference independence. On the other hand, cortical imaging methods have more potential to make use of information about the volume conductor to improve the accuracy of cortical potential estimates. Actually, one may think of high resolution EEG methods on a continuous scale with local Laplacians as entirely model-independent, spline-Laplacians as minimally model-dependent, smoothed cortical imaging methods as moderately model-dependent, and unsmoothed cortical imaging as strongly model-dependent. At this stage of our understanding of brain sources and head volume conductors, it makes sense to apply methods from different parts of this spectrum to the same data. Only those conclusions about brain function which are robust to choice of method can be considered reliable.

Simulations of Laplacian and cortical imaging methods

We have discussed two fundamentally different categories of approach to high resolution EEG, surface Laplacians and cortical imaging. Here we examine relationships between these two approaches, based on theoretical arguments, computer simulations, and (in the next section) actual EEG data. The physical bases for the relationship between cortical potential and scalp surface Laplacian have been discussed in Nunez (1981) and Katznelson (1981a), in which the following approximate relationship is implied:

$$V_B \sim V_S + A_{KS} L_S \quad (1)$$

Here the variables V_B and V_S are potentials at various tangential locations over the inner and outer surfaces of the skull, respectively. L_S is the negative surface Laplacian (measured in $\mu V/cm^2$). We regard these variables as potentials and Laplacians averaged

over surface areas of electrodes, rather than potentials at points. In the case of a homogeneous skull, the parameter A_{KS} (cm^2) may be crudely approximated by

$$A_{KS} \sim d_K d_S (\rho_K / \rho_S) \quad (2)$$

where d_K and d_S are skull and scalp thickness and ρ_K and ρ_S are skull and scalp resistivities, respectively. The validity of Eq. 1 is dependent on Ohm's law in the skull and the fact that skull resistivity is much larger than that of the brain (assumed here to roughly equal scalp resistivity). The latter condition assures that skull current is mostly perpendicular to its surface. It should be emphasized that Eq. 1 is independent of the nature and location of sources or assumptions about the head volume conductor, except to the extent that these variables influence the direction of skull current (believed to be a very minor effect in the case of cortical sources). While Eq. 1 is only an approximation, its apparent robust character when applied to the head volume conductor provides the primary motivation for the use of the surface Laplacian in EEG. Eq. 2 may be a reasonable approximation at relatively large scales (e.g., 1 or 2 cm) in the case of homogeneous skull. This latter condition is questionable; however, the approximation of Eq. 2 is evidently not required in most applications.

Simulations predict that potentials vary relatively slowly through scalp thickness. This is illustrated in Fig. 5, which shows the theoretical potential due to a radial dipole in the cortex as a function of radial location through CSF, skull, and scalp. Thus, measured scalp potential approximates outer skull surface potential V_S. The closeness of the inner skull surface potential V_B to cortical potential V_C depends on CSF thickness, dipole orientation and other factors. For example, the difference between V_C and V_B is expected to be larger for tangential dipoles than radial dipoles due to enhanced tangential CSF current generated by tangential dipoles. However, when CSF thickness is relatively small (e.g., $\sim$ 0.5–1 mm), our simulations indicate that V_B approximates V_C reasonably well.

Thus, if one records scalp potential ($\sim V_S$) and estimates scalp Laplacian (L_S), cortical potential ($\sim V_B$) may be crudely estimated from Eqs. 1 and 2, provided that the resistivity ratio ρ_K/ρ_S, scalp and skull thicknesses are known. However, this step, which involves the very rough approximation of Eq. 2, is evidently not necessary in most applications. One reason is that the ratio of scalp to cortical potential is typically at least 2–4 in the case of widely distributed cortical sources and even larger for localized cortical sources (Nunez 1981, 1990b). These data which have been established in EEG for several decades (refer, for example, to Penfield and Jasper 1954) imply that the second term on the right side of Eq. 1 is often much larger than the first, i.e., cortical potential is roughly proportional to scalp Laplacian at scales in the 1–2 cm range or larger. Furthermore, the estimate of cortical potential pattern obtained from the 2nd term in Eq. 1 is independent of head model, except that variations in resistivities or thicknesses will, of course, cause some distortion of the cortical potential estimate.

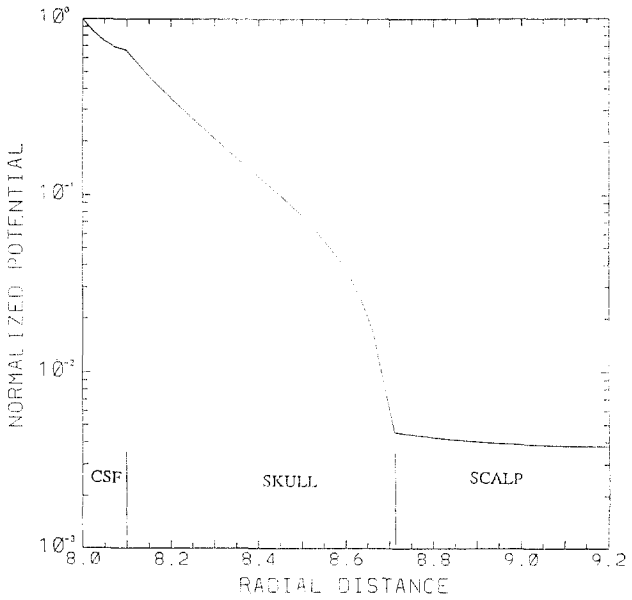

Fig. 5. A 4-concentric sphere model (including a 1 mm thick layer of CSF) is used to calculate the attenuation of potential with radial distance (r in cm) above a radial dipole. Here the dipole is located in the cortex (r = 7.8), and potential is normalized with respect to its magnitude at the inner CSF surface (r = 8.0). Potential falls through the CSF; however, if CSF forms a thin layer as shown here, this drop is not large. Potential falls off quite rapidly through the skull ($8.1 \leqslant r \leqslant 8.7$) to a value of about 1/500 that of its value at the inner CSF surface. By contrast, potential attenuation through the scalp is quite small. In this simulation, scalp and brain resistivities are equal, CSF resistivity is 1/5 that of the brain, and skull resistivity is 80 times that of the brain. The qualitative features of this plot are not critically dependent on these assumptions, however. When a large dipole layer is active in the cortex, the potential at any radial location is due to the linear superposition of many sources. In this case, the total attenuation of potential above the layer is much less, i.e., the predicted ratio of cortical to scalp potential generally lies in the range of about 2–6 if 10 or more cm^2 of free cortical surface is active (Nunez 1981, 1990b).

The expected close relationship between analytic scalp Laplacian and analytic cortical potential in the case of distributed neocortical sources is illustrated in Fig. 6. The source distribution in the upper left plot results in the scalp potential map (analytic) at the upper right, calculated with the 3-sphere model (no CSF). Cortical surface potential (lower left) and scalp Laplacian (lower right) are both calculated in the same manner, showing that scalp Laplacian closely approximates cortical potential, but scalp potential is a poor representation of cortical potential in this idealized (3-sphere) model.

Scatter diagrams of cortical potential versus scalp potential and cortical potential versus scalp Laplacian are shown in Fig. 7. These are obtained by sampling 640 points on inner and outer spheres so that values of these variables at the same tangential locations are directly compared. The plots on the upper row correspond to the example in Fig. 6 (no CSF), whereas plots on the lower row are obtained from the same source distribution (upper left of Fig. 6) with the 4-sphere model and CSF thickness = 1 mm. Correlation coefficients are shown in the lower right corner of each plot, indicating how much more closely scalp Laplacian approximates cortical potential than does raw scalp potential. However, as CSF thickness further increases, both scalp potential and scalp Laplacian become progressively less accurate measures of cortical potential (i.e., potential at the inner surface of the CSF layer). For example, if CSF thickness is 2 mm, the scalp potential/cortical potential and scalp Laplacian/cortical potential correlation coefficients drop to 0.33 and 0.52, respectively for this source distribution, due to additional spreading of source currents by the CSF. This result may be of particular interest in clinical EEG studies since CSF thickness increases in normal aging from 0.5 mm or less for subjects in their mid 20s to over 5 mm in normal subjects aged 80 and over (De Leon et al. 1986; Helme 1991). These simulations are based on an assumed CSF resistivity which is 20% of that of brain tissue. If a CSF resistivity equal to 40% of brain tissue resistivity were used in the simulations, our results for 0.5–2 mm thickness would be applicable to CSF thicknesses of 1–4 mm, due to reduced current spread in the CSF.

The slopes of the linear regression lines in the plots of the left column of Fig. 7 are measures of the average ratio of cortical to scalp potential. The slopes are

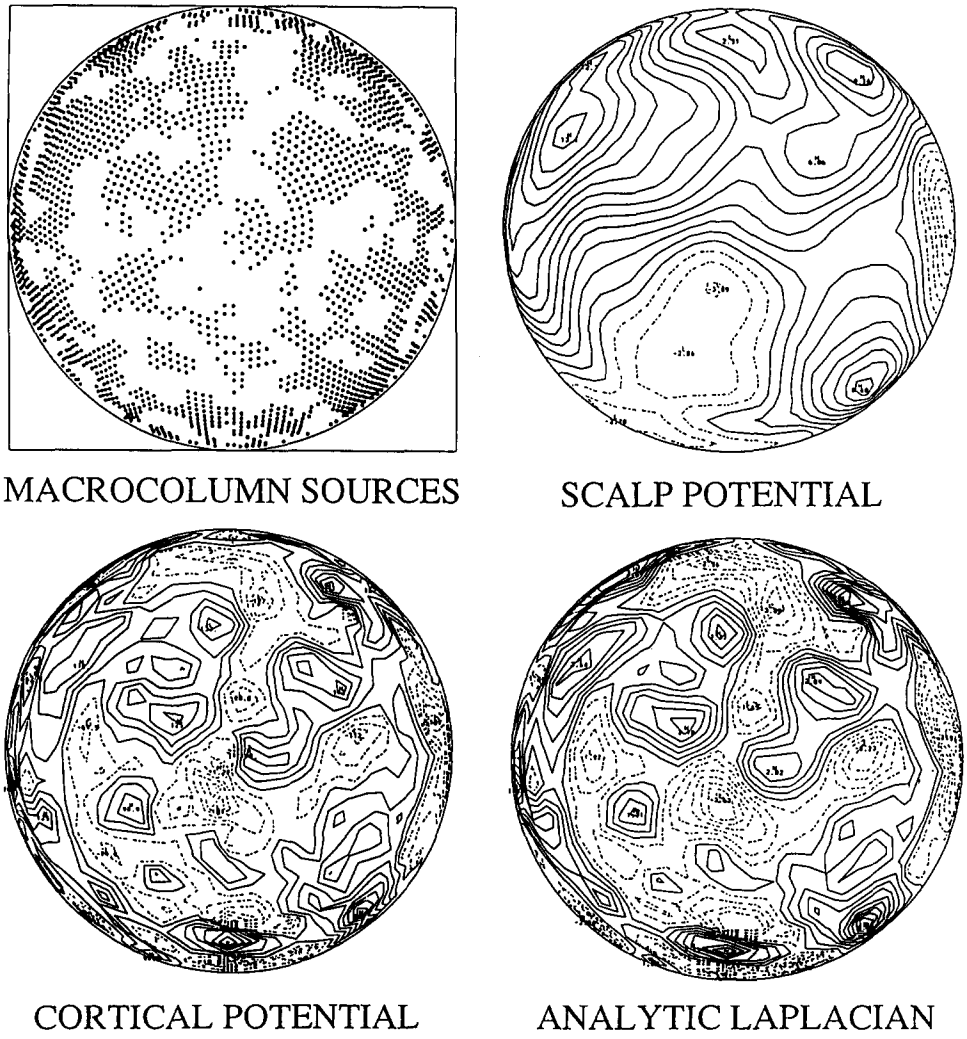

Fig. 6. Upper left: an assumed distribution of 4200 radial dipoles with source strength distributed between + and −200 μV. Filled spaces are positive sources, blank spaces are negative sources. Upper right: analytic potential on the outer sphere (scalp) of the 3-sphere model (no CSF) provides a relatively poor representation of cortical source pattern (upper left) or analytic cortical potential (lower left). However, analytic scalp Laplacian (lower right) provides an excellent estimate of cortical potential. Correlation coefficients are shown in Fig. 7.

roughly in the range 15–25 in these examples, based on the moderately clumped source distribution of Fig. 6. Slopes of the regression line are strongly affected by the degree of correlation (i.e., the "clumpiness") of the sources. In the case of random sources, slopes can be greater than 100, as in the case of the single dipole source of Fig. 5. By contrast, highly clumped sources of the same sign result in slopes in the general range of about 2–6, as discussed in Nunez (1981, 1990b). The former examples are apparently reasonable models for focal epilepsy; the latter examples appear to be much closer to spontaneous EEG (Nunez 1981).

In order to study the robustness of high resolution methods, the spline surface Laplacian estimates developed at Tulane University (Nunez et al. 1991; Law et al. 1993) are compared to cortical images estimated with a sophisticated algorithm developed at the Swinburne Centre for Applied Neurosciences in Melbourne, Australia (Cadusch et al. 1992). Both the Laplacian algorithm and the Australian cortical imag-

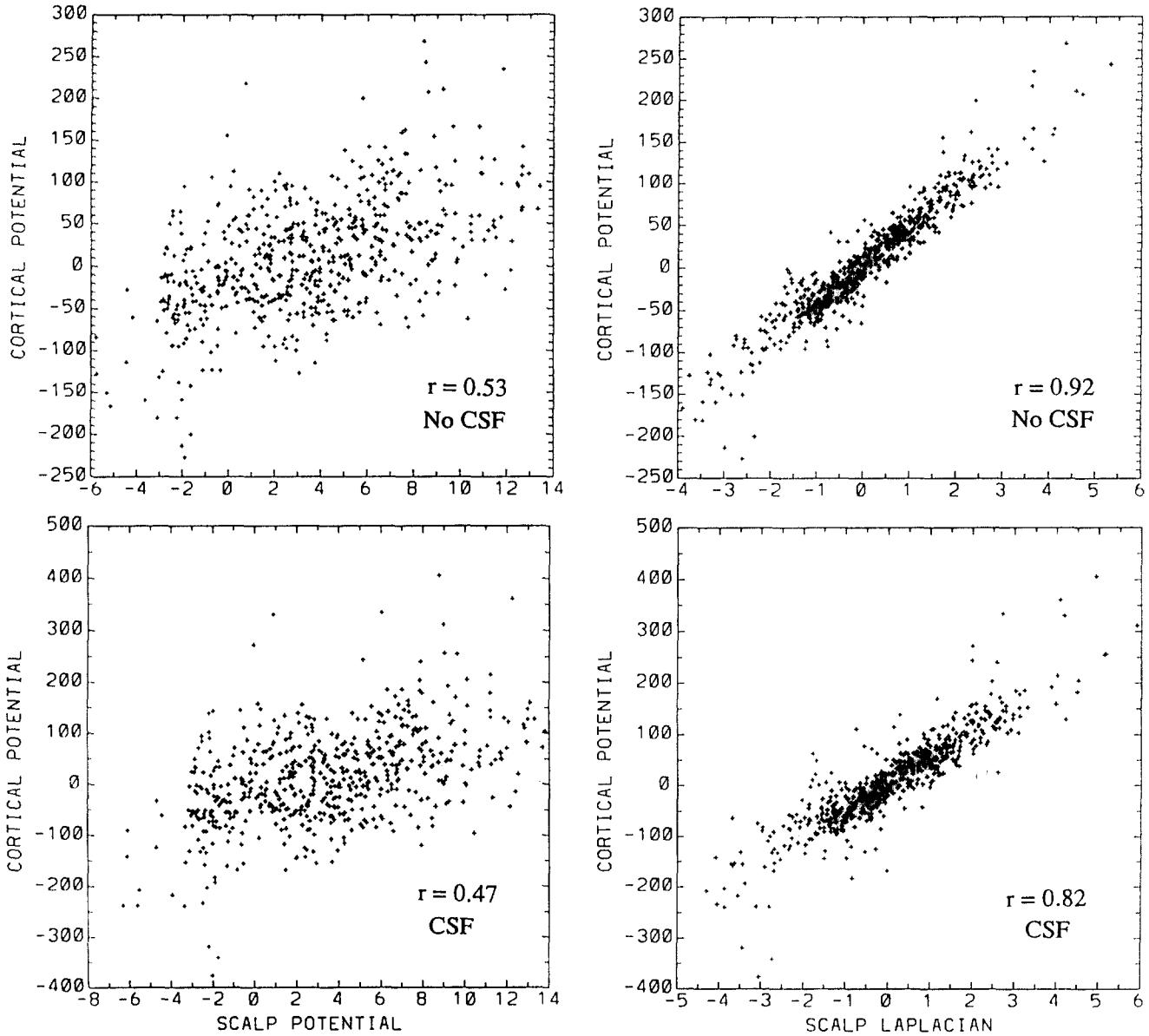

Fig. 7. Theoretical scatter plots showing cortical potential versus analytic scalp potential (left column) and analytic scalp Laplacian (right column) for the moderately clumped source distribution of Fig. 6. The scatter diagrams were obtained by sampling pairs of potentials (and Laplacians) on the surfaces of the inner sphere (cortex) and outer sphere (scalp) at 640 tangential (e.g., angular) locations. Correlation coefficients are shown in lower right corners of each plot. Cortical source magnitudes vary between ± 200 μV (potential across the macrocolumn scale cortical dipole layers). Potentials (with respect to infinity) are expressed in μV; Laplacians are $\mu V/cm^2$. Cortical potentials tend to have large magnitudes near large clumps (of the same sign) due to superposition of fields generated by individual macrocolumn dipoles (refer to Nunez 1990b for discussion of "macrocolumn sources"). The plots in the upper row are obtained from a 3-sphere model (no CSF); plots in the lower row are obtained using a 4-sphere model with CSF thickness = 1 mm.

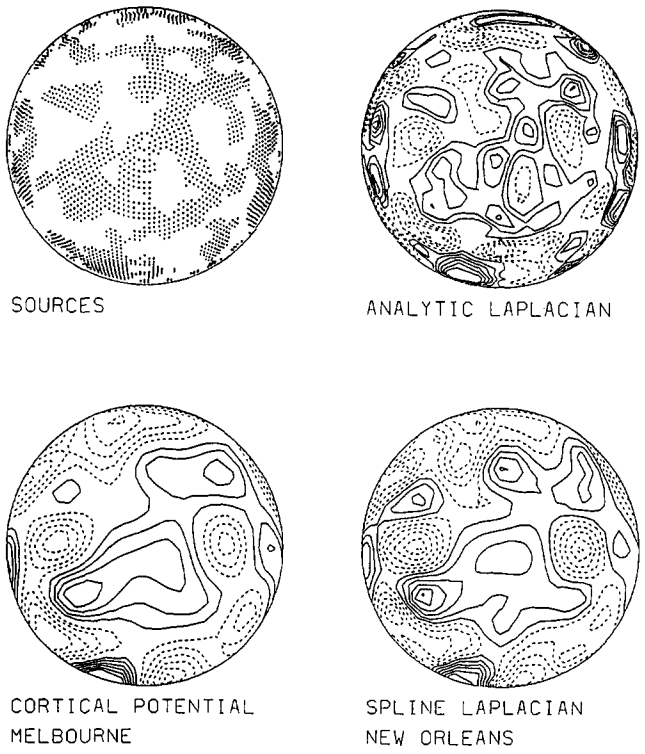

Fig. 8. Comparison of New Orleans and Melbourne methods. Upper left: source distribution, identical to that used in Figs. 1 and 4. Upper right: actual (analytic) Laplacian. Lower left: estimate of cortical surface potential based on 64 scalp potential samples using cortical imaging methods developed by the Melbourne group with smoothing factor $\lambda = 10^{-9}$. Lower right: estimate of surface Laplacian based on the same samples using the method developed by the New Orleans group.

ing algorithm use spline functions so that all estimates are "global," i.e., estimates of Laplacian or cortical potential at each location depend on the potentials recorded at all electrodes, rather than only on nearest-neighbor electrodes as, for example, in the case of the 5-electrode Laplacian (Hjorth 1975). The Laplacian methods involve interpolation in 3-dimensional space (Law et al. 1993), whereas the Australian interpolation is on a sphere (Wahaba 1981). The Laplacian methods are independent of head model, except for the original choice of spline and the assumption of a spherical scalp surface. The Laplacian methods are an extension of earlier spline-Laplacian methods developed by the French group which use interpolation in a plane (Perrin et al. 1987a,b; Nunez 1988, 1989a) or on a spherical surface (Perrin et al. 1989). The Australian cortical imaging method uses a 3- or 4-concentric sphere model. Even though these two approaches have quite different theoretical bases, the resulting predictions of cortical potential at moderate scales ($\sim$ 2–3 cm or larger) are quite similar when applied to simulated data as illustrated in Fig. 8.

The cortical image estimates are predictions of cortical surface potential, given a known scalp distribution and volume conductor (Cadusch et al. 1992). The method illustrated here involves the same physical principles as earlier, crude deconvolution methods (for example, Nunez 1987a). However, the new cortical imaging methods are more sophisticated and robust in that they include an explicit smoothness criterion to allow for noisy data and an imperfect volume conductor model. Thus, the relationship of the new cortical imaging methods to earlier spatial deconvolution is somewhat analogous to the relationship of the new global spline-Laplacian methods to earlier nearest-neighbor Laplacians as described by Hjorth (1975) and Nunez (1981), for example.

In the case of the simple cortical source patterns, which involve either isolated dipoles or a few "clumps" (i.e., regions of highly correlated sources, not shown), both the Laplacian and cortical imaging methods yield nearly identical patterns. In the case of the more complicated source distribution of Fig. 8, there are only minor differences in predicted patterns. These illustrations demonstrate the practical equivalence of two high resolution methods based on quite different theoretical approaches, at least for simulated sources inside 3- or 4-sphere models. It should be noted that both Laplacian and cortical imaging methods cited here are nearly independent of actual brain to skull resistivity ratio. For example, if we carry out forward solutions (calculation of scalp potential due to known sources), using resistivity ratios in the range of 5–500, both methods provide accurate estimates of cortical potential patterns (i.e., relative, but not absolute, magnitudes), even though the cortical imaging algorithm is based on a skull to brain resistivity ratio of 80. We have carried out many simulations involving different patterns of distributed sources. The correlation coefficients between the spline-Laplacians and cortical images varied between 0.8 and 0.95 in these simulations.

Spatial filtering properties of Laplacians and cortical images

Another way to illustrate the differences between high resolution and conventional EEGs is by their different spatial filtering properties. It is well known in clinical EEG that different choices of reference electrode emphasize certain sources at the expense of others. Thus, the choice of reference electrode (or particular bipolar montage) can be viewed as a spatial filter with respect to source location. An extension of this idea is that of a spatial filter with respect to the size of the correlated source region (Nunez 1988).

In order to illustrate the spatial filtering properties of various methods, we make use of natural functions for spherical surfaces known as the spherical harmonics $Y_{nm}(\theta, \phi)$. Here θ and ϕ are the usual spherical

coordinates, essentially latitude and longitude in the case of the earth's surface. (Refer to the spherical coordinate system shown in the upper left corner of Fig. 9.) For illustrative purposes, we consider the north pole to be at C_z. The index n can take on any integer value from 0 to ∞. The index m can take on any value from $-n$ to $+n$. The Y_{nm}s form an orthogonal set of (many) functions on the surface of a sphere. The larger the index n, the higher the "spatial frequency" in the θ direction. The larger the index m, the higher the "spatial frequency" in the ϕ direction. We put the words "spatial frequency" in quotes since this term is not precisely defined for non-sinusoidal functions. However, the general intuitive idea of spatial frequency

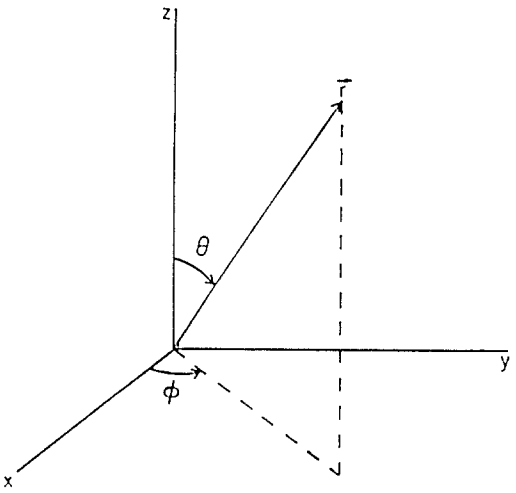

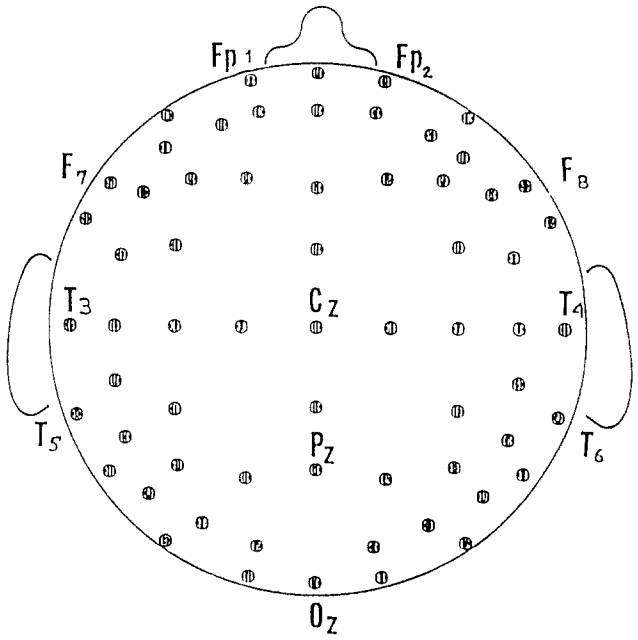

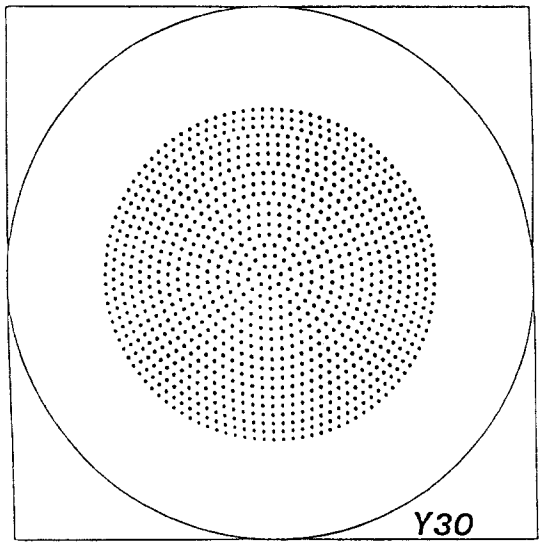

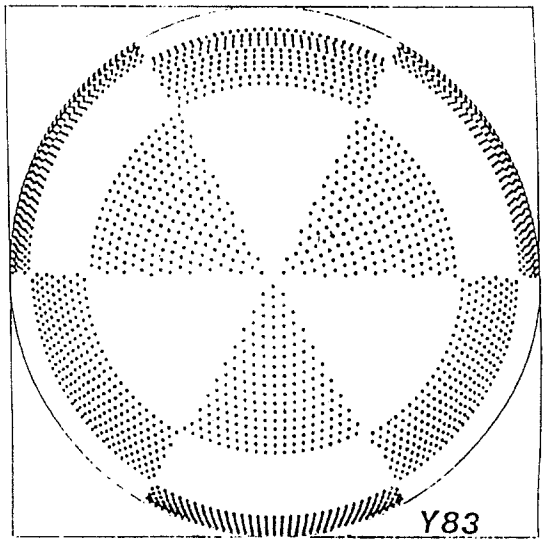

Fig. 9. Nearly any function $V(\theta, \phi)$ (e.g., potential, source magnitude) on a spherical surface can be represented as the series

$$V(\theta, \phi) = \sum_{n=0}^{\infty} \sum_{m=-n}^{+n} A_{nm} Y_{nm}(\theta, \phi)$$

which is analogous to the usual Fourier series with time as a single independent variable. Here the two angles θ and ϕ are the independent variables. The usual spherical coordinate system is shown in the upper left corner. The Melbourne electrode array, consisting of spring loaded electrodes in a spherical helmet, is shown at the upper right. These positions are also used for simulated data. The coordinate system is oriented so that the z-axis passes through C_z. Examples of the spherical harmonics $Y_{nm}(\theta, \phi)$ are shown in the lower row (n = 3, m = 0 and n = 8, m = 3). The indices n and m indicate "spatial frequencies" in the θ and ϕ coordinates, respectively. In these plots, the perspective is from the upper pole ($\theta = 0°$) of the sphere, the region $0 \leqslant \theta \leqslant 90°$ is shown, and ϕ varies from 0 to 360° around the circular regions shown. Source strengths vary continuously over the sphere with positive sources indicated by filled spaces and negative sources by empty spaces. All spatial patterns shown here can be represented as a superposition of spherical harmonics with different weighting coefficients A_{nm}.

applies very well to these functions as illustrated in Fig. 9 and by the approximate relations:

$$k_\theta = \frac{n+1-|m|}{2\pi R} \qquad n = 0, \infty$$
$$k_\phi = \frac{|m|}{2\pi R \sin\theta} \qquad m = -n, n \tag{3}$$

Here R is sphere radius and k_θ, k_ϕ are spatial frequencies (cycles/cm) in the latitudinal and longitudinal directions, respectively. For example, with a sphere radius (brain) of R = 8 cm, $Y_{10}(\theta)$ has a spatial wave length of about 25 cm and $Y_{80}(\theta)$ has a wave length of about 6 cm. The spherical harmonic functions Y_{nm} are natural functions for systems with spherical geometry in the same way that sines and cosines apply naturally to 1-dimensional systems. For example, it has been shown that the spatial principal components of any process defined on a spherical surface for which

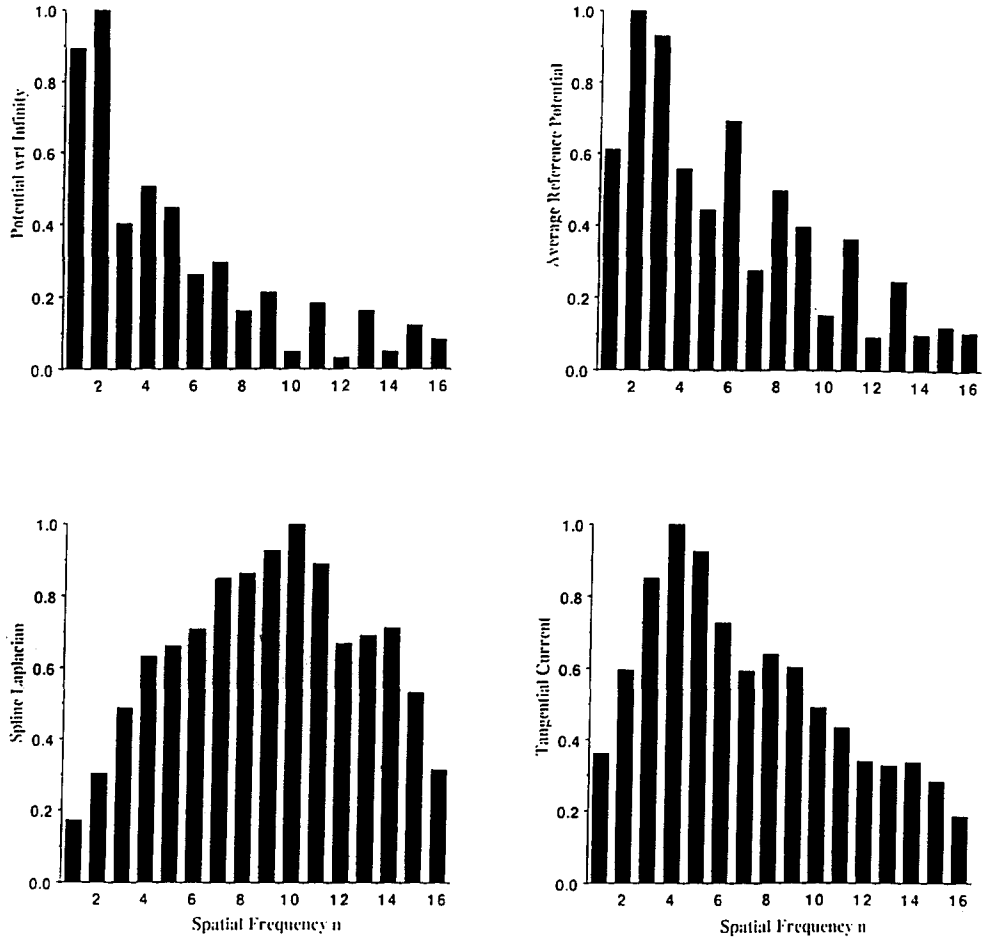

Fig. 10. The sensitivity of various estimation methods to different spatial frequencies, based on sampling of potential at the 64 scalp locations, as shown in Fig. 9. The bars represent normalized RMS measures. The horizontal scale is the n index, corresponding to different spatial frequencies of the sources in the θ direction. For each n, the source distribution is averaged over spatial frequencies in the ϕ direction, i.e., source distribution

$$S_n = \sum_{m=-n}^{+n} Y_{nm}(\theta, \phi).$$

For each estimate, RMS values (based on 64 sample locations) are normalized to one at the n yielding maximum magnitude (only n > 0 are shown here). In all plots, somewhat uneven distributions result from discrete sampling. Upper left: raw scalp potential (with respect to infinity) is shown to be most sensitive to low spatial frequencies (e.g., n = 0–2). This spectrum can be altered by different choices of reference. Lower left: the spline-Laplacian yields a much more uniform sensitivity to spatial frequency than does the raw potential. However, it is much less sensitive to very low spatial frequencies. Lower right: the tangential scalp current (obtained from the New Orleans spline algorithm) provides a rough estimate of results expected from close bipolar electrodes. The response of this measure is non-uniform and maximum at the spatial frequency n = 4. Upper right: the average reference potential is most sensitive to spatial frequencies n = 2 and 3. As such it represents somewhat of an intermediate case between potential with respect to infinity and tangential scalp current density. These plots summarize some of the reasons why different measures (reference, bipolar, Laplacian) are sensitive to sources at different spatial scales. They show why the Laplacian, which exhibits a more uniform response at different spatial frequencies, is generally a more accurate measure of cortical source distribution. Another advantage of the Laplacian (not illustrated here) is its independence of the reference electrode.

the correlation between any two points is only a function of distance must be the spherical harmonics (Silberstein and Cadusch 1992). Various other applications of the spherical harmonics in EEG have also been proposed (Nunez 1981; Katznelson 1981b; Shaw 1991; Koles and Soong 1992; Lagerland et al. 1992).

The spatial filtering properties of various methods are illustrated by assuming that cortical source distribution is composed of functions $S_n = \sum_{m=-n}^{+n} Y_{nm}$ for different indices (n). These functions represent different spatial frequencies in the θ direction, averaged over spatial frequencies in the ϕ direction. The predicted scalp potential at 64 locations is then calculated using the standard 3-concentric sphere model of the head (Nunez 1981). The 64 scalp potential values are submitted to the spline algorithm which obtains estimates of scalp tangential and skull radial current density, the former closely associated with bipolar recordings and the latter being essentially the surface Laplacian. The RMS magnitudes of the outputs of this algorithm then provide a general idea of the average scalp magnitude of each EEG measure to be expected from each S_n source distribution. That is, an estimate of the sensitivity of each measure is obtained as a function of spatial frequency as shown in Fig. 10.

Raw scalp potential (upper left) is shown to be most sensitive to very low spatial frequencies (n = 0–2). This result (together with reference electrode effects not considered here) indicates why conventional methods provide such poor localization of isolated sources. The general spatial filtering properties of bipolar recordings (with close electrodes) are shown in the scalp tangential current plot at lower right. Actual sensitivity to specific sources depends, of course, on the orientation of electrode pairs; however, the plot can be viewed as an overall average over many bipolar pairs. Scalp tangential current is seen here to be more sensitive to higher spatial frequencies (peak at n = 4) than raw

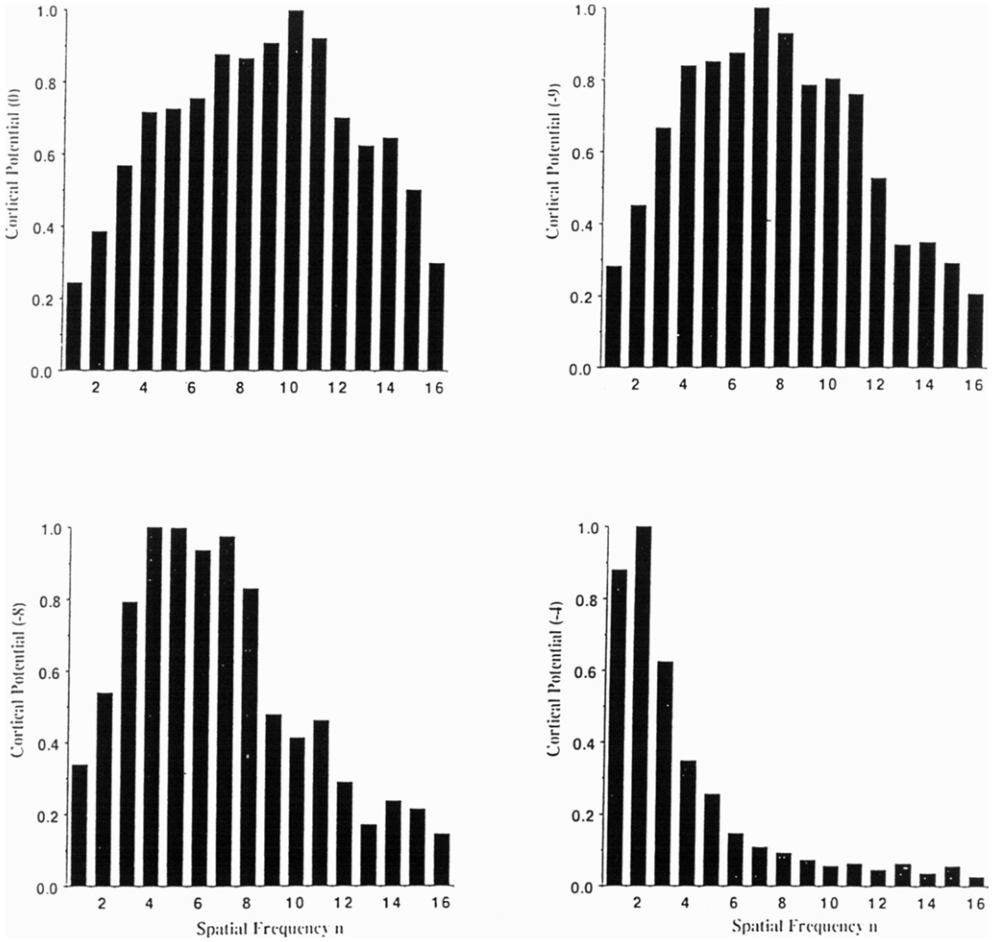

Fig. 11. Spatial filtering properties of the cortical imaging method developed by the Melbourne group. Similar to Fig. 10, except that each of the 4 plots refers to an estimate of cortical surface potential obtained with different smoothing parameters λ. Upper left: $\lambda = 0$. Upper right: $\lambda = 10^{-9}$. Lower left: $\lambda = 10^{-8}$. Lower right: $\lambda = 10^{-4}$. The plots with minimal smoothing result in spatial frequency sensitivity similar to the Laplacian (refer to Fig. 10). As smoothing is increased, less and less detail becomes evident in estimated cortical potential. Very large smoothing produces a spatial frequency selectivity similar to raw potential (upper left corner of Fig. 10). When smoothing is too small, finer details become unreliable due to noisy data and/or uncertainty in the volume conductor model.

potential measures. Average reference potential is most similar to tangential scalp current (upper right). The spline-Laplacian estimate (lower left), which provides a reasonably accurate representation of the actual (analytic) Laplacian, is approximately equally sensitive over a broad range of spatial frequencies (roughly n = 3–15). As such, it is sensitive to the spatial frequency range where raw potential is insensitive. Thus, one may conclude that raw potential and Laplacian estimates provide somewhat complementary but partly overlapping information, with the former mainly good for studying very large scale (low spatial frequency) sources, provided reference electrode distortion is not too severe.

The spatial filtering properties of estimates of cortical surface potential obtained with spline-based cortical imaging methods are shown in Fig. 11 for various values of the smoothing parameter λ. Large values of λ (oversmoothing) result in very low-pass filtering, similar to raw potential. Undersmoothing ($\lambda \rightarrow 0$) results in apparently desirable filtering characteristics. However, it must be kept in mind that the spectrum of Fig. 11 is based on known volume conductor characteristics. When applied to real data, the head volume conductor can be expected to have characteristics that lie within some range of uncertainty so that an intermediate value of λ is apparently appropriate. The choice of smoothing $\lambda = 10^{-9}$ (upper right) closely matches the spatial filtering properties of the New Orleans spline-Laplacian.

Experimental comparisons of Laplacians and cortical imaging

We have applied spline-Laplacian and cortical imaging methods to two kinds of experimental data, steady-state visual evoked potentials (SSVEP) and spontaneous EEG (alpha). The former data were obtained in various cognitive studies in which continuous sinusoidal driving in both task and non-task conditions allows for the study of scalp magnitude and phase distributions in narrow frequency bands (Silberstein et al. 1992). The motivations for this approach include the elimination of nearly all artifacts in these narrow bands and the creation of stable spatial patterns during resting (e.g., control) states, which change significantly during cognitive task performance. Spontaneous EEG was recorded during the same recording sessions. We report here on spatial patterns obtained from data obtained in one subject which is representative of data obtained in several other subjects. Since actual source distributions are unknown, emphasis is placed on comparisons between spline-Laplacians and cortical images in this section.

The steady-state visually evoked potentials were elicited by spatially uniform sinusoidal stimuli at frequencies typically in the 8–23 Hz range (refer to Regan 1989 for general discussion). Scalp potentials were recorded with a 64-channel system developed by the Melbourne group. Spring loaded electrodes are fitted through a hard, shielded helmet. Electrode placement and impedance check typically require about 20 min. A balanced, non-cephalic (neck) reference was used, as described in Stephenson and Gibb (1951). Several minutes of spontaneous EEG were also obtained in each subject. Here we report only on alpha band activity obtained with eyes closed and eyes open SSVEP during the "non-task state."

Fourier transforms of wave forms obtained at each of the 64 electrode sites yielded 64 real and 64 imaginary coefficients at the driving frequency, thereby preserving relative phase information. The sets of real and imaginary coefficients were submitted to both the spline-Laplacian and cortical imaging algorithms. Thus, each SSVEP epoch of length T yielded 3 sets of Fourier coefficients corresponding to raw potential (i = 1), surface Laplacian (i = 2) and cortical potential estimate (i = 3) at the driving frequency. Note that 1/T Hz frequency resolution corresponds to Fourier transform epochs of T seconds duration. The SSVEP data were typically viewed over 250 sec duration, i.e., in a narrow band of 0.004 Hz centered at the driving frequency.

Real and imaginary patterns obtained from Laplacian and cortical imaging algorithms were compared with each other and with raw potential by calculating correlation coefficients. We have made several hundred such comparisons with both SSVEP and spontaneous EEG data. The SSVEP correlations involve long time records and narrow frequency bands, whereas the spontaneous EEG correlations involve a variety of frequency bands (e.g., 0.5–4 Hz). Correlation coefficients between spline Laplacian and cortical image estimates ($\lambda = 10^{-9}$) are nearly all in the 0.75–0.95 range. By contrast, correlation coefficients between either Laplacians or cortical images and raw scalp potential are typically in the 0.3–0.5 range. These results are generally consistent with the simulation studies illustrated in Fig. 7.

Real and imaginary spatial patterns of alpha rhythm based on averages of twenty-two 1 sec epochs were obtained by submitting the 64 averaged real and 64 averaged imaginary Fourier coefficients to the spline-Laplacian algorithm and cortical imaging algorithm. (Real and imaginary coefficients were rotated for each 1 sec epoch so that Pz had zero phase for each epoch.) Since a large part of power in the alpha rhythm is in a narrow band around 10 Hz, these patterns of Fourier coefficients are very similar to typical "snapshots" of alpha potential distribution over the scalp at fixed times.

Magnitude and phase plots were also obtained from the usual relations between (magnitude, phase) and (real, imaginary) parts of the Fourier transform, i.e.,

$$\text{Mag}_{ij} = \left(\text{real}_{ij}^2 + \text{imag}_{ij}^2\right)^{1/2} \tag{4}$$

$$\text{Phase}_{ij} = \tan^{-1}\left(\frac{\text{imag}_{ij}}{\text{real}_{ij}}\right) \tag{5}$$

The subscripts i = 1, 2, 3 and j = 1, 64 refer to the type of estimate and electrode position, respectively. In the case of alpha rhythm, epoch lengths of T = 1 sec were used so as to obtain a frequency resolution of 1 Hz. That is, amplitude and phase of 10 Hz activity include contributions mostly from the band between 9.5 and 10.5 Hz. We chose a relatively broad bandwidth for the spontaneous activity because of the well-known tendency of the peak alpha frequency to drift over a frequency range of ± 0.25 to ± 0.5 Hz during resting states (Nunez 1981).

Magnitude and phase plots for the 22 sec period of alpha rhythm are shown in Fig. 12. The left column is obtained from raw potential data. The middle column contains corresponding Laplacian magnitude and phase plots. The right column shows magnitude and phase

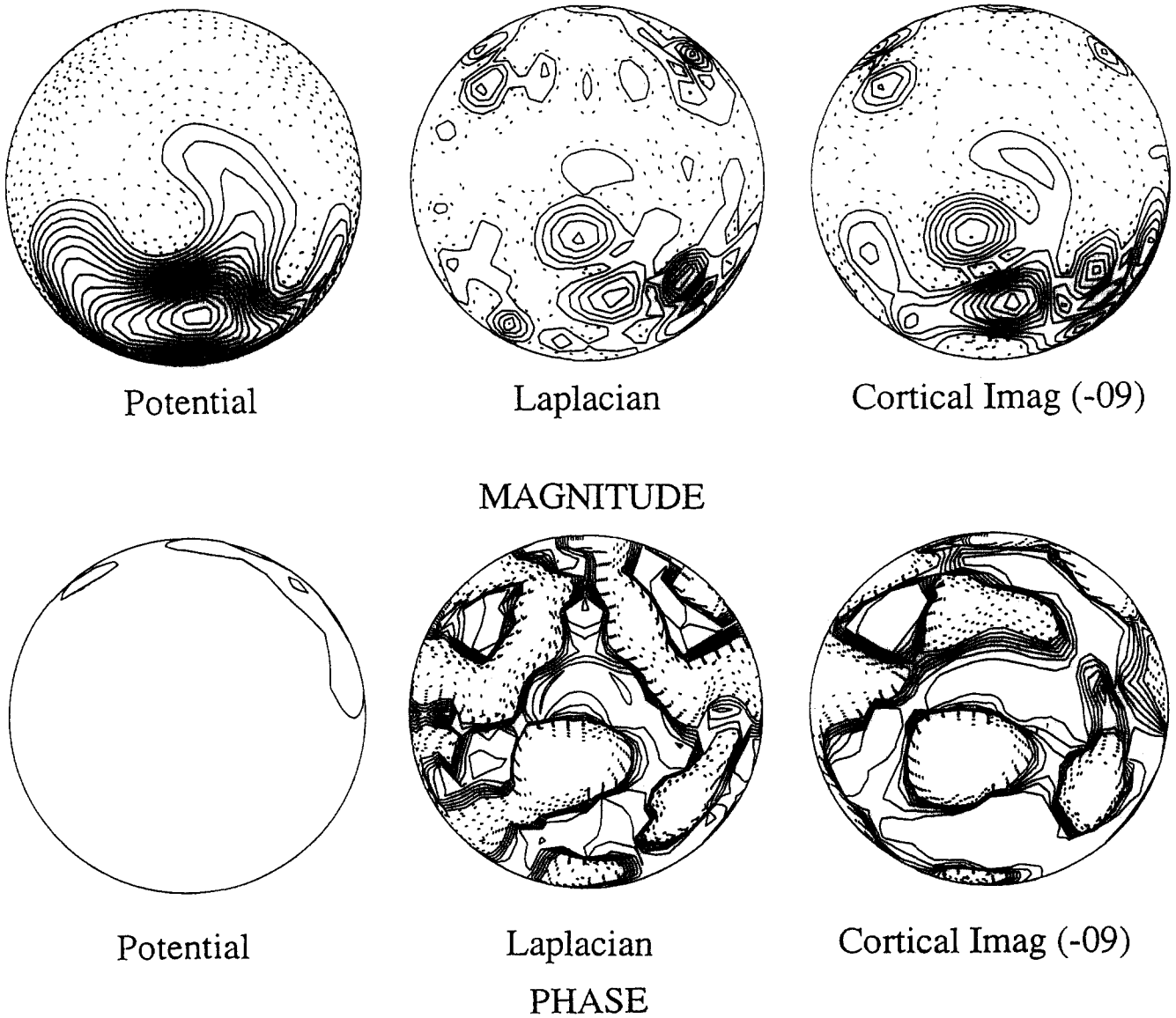

Fig. 12. Magnitude and phase plots for a 22 sec period of alpha rhythm. The left column is obtained from unprocessed potential data (non-cephalic reference). The middle column shows corresponding Laplacian magnitude and phase plots. The right column is the cortical image estimate. Above average magnitudes are plotted as solid lines, below average are dotted lines (interval 0.43 μV). Maximum potential in the 1 Hz band is 8.1 μV (maximum potential over the entire alpha band is about 40 μV). Laplacian magnitude contour intervals are 0.43 $\mu V/cm^2$. The phase plots are cosine (phase) with zero phase chosen arbitrarily at Pz. Both potential and Laplacian phase plots have contour intervals of 0.15 (dimensionless).

plots obtained from the cortical imaging algorithm. We have produced approximately 100 of these plots in several subjects, including averages over various periods as well as single (1 sec) epoch plots. While this paper is not a study of alpha rhythm characteristics, we note the following general features common to most of our maps:

(1) Scalp potential magnitudes based on averaged data are largest over posterior regions; however, individual 1 sec epochs often suggest significant correlated electrical activity in central and frontal cortex. This is illustrated by the magnitude and phase plots for 4 successive seconds of alpha rhythm shown in Fig. 13 (scalp potential) and Fig. 14 (spline-Laplacian).

(2) Magnitude and phase plots of Laplacian or cortical image estimates show a "quasi-stable" structure. In order to quantify pattern stability, we first obtained template magnitude and phase plots based on averages over 3 min of data. These template maps were similar to the 22 sec averaged maps of Fig. 12 (middle column). The templates were compared to magnitude and phase estimates based on 180 successive 1 sec epochs of the same data. Random magnitude and phase correlations phase correlations can vary between -1 and $+1$. Actual EEG magnitude correlations obtained in this manner varied mostly between 0.3 and 0.7. Phase correlations were mostly in the 0.1–0.6 range. Thus, significant second-to-second pattern variability was observed. However, these patterns were far from random, with many 1 sec epochs matching the template reasonably well. Magnitude and phase correlations based on much longer epochs (e.g., 1 min) are typically greater than 0.9, i.e., as the epochs become longer spatial structure becomes more stable."

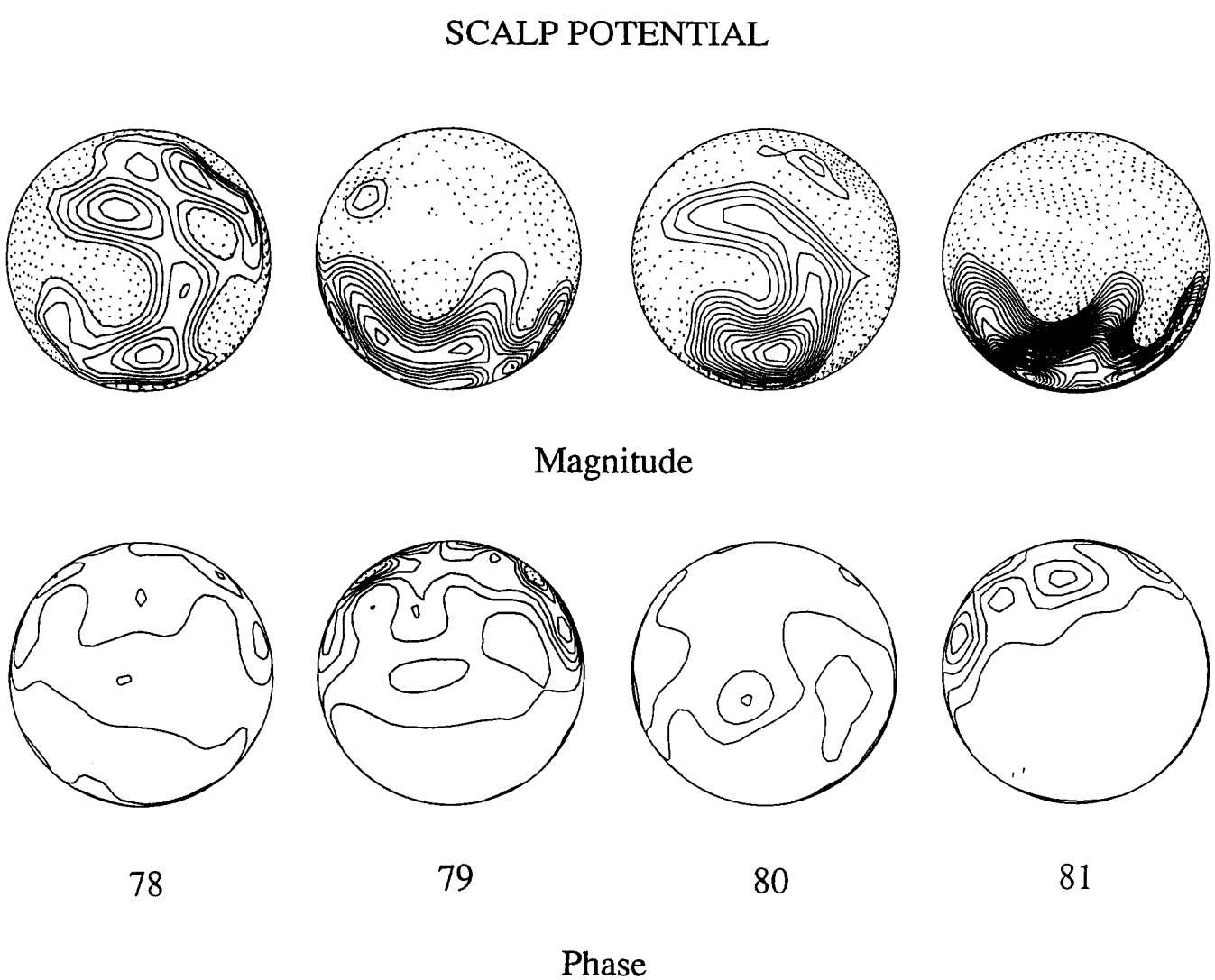

Fig. 13. Magnitude and phase plots of raw scalp potential for 4 successive sec of alpha rhythm (epochs 78–81 of the 22 epochs of Fig. 12). These epochs were chosen arbitrarily, except for obtaining successive epochs of high amplitude alpha. Maximum potential magnitude in the 1 Hz band centered at 10 Hz is 6.7 μV. Cosine (phase) plots have intervals of 0.15, and cosine (phase) at Pz is chosen to be 1, as in Fig. 12.

(3) Laplacian and cortical image magnitudes (which are mostly quite similar to each other) have widespread local maxima over both anterior and posterior cortex. These may be due to local regions of more highly coherent (e.g., "clumped") sources as illustrated by the simulations depicted in Figs. 1, 2, 4 and 6. Our data suggest that the well-known predominance of alpha rhythm over posterior scalp regions may be mostly due to more and/or larger regions of coherent source activity in posterior cortex, but that significant frontal sources also occur. Physiological changes that interrupt this coherent activity (perhaps eye opening) should cause a significant reduction in scalp potential magnitude, based on both long-held notions about EEG "synchrony" and our simulations using known sources.

(4) Scalp potential phase plots show relatively gradual phase changes, nearly always less than 90° over the entire electrode array and often much less than this. Phase changes are most gradual over regions of large scalp magnitude, but generally show larger gradients over regions of lower scalp magnitude, as shown in Fig. 13. In cases of larger relative scalp magnitudes in frontal regions, phase changes are very gradual over the entire scalp. This is illustrated by two of the 1 sec epochs shown in Fig. 13, in which scalp potential phase changes by only about 45° over the entire electrode array.

(5) By contrast to the relatively gradual changes of scalp potential phase, Laplacian (or cortical image) phase nearly always exhibits multiple abrupt phase changes of 180° over a few centimeters, as illustrated in both Figs. 12 and 14. Correspondence between bound-

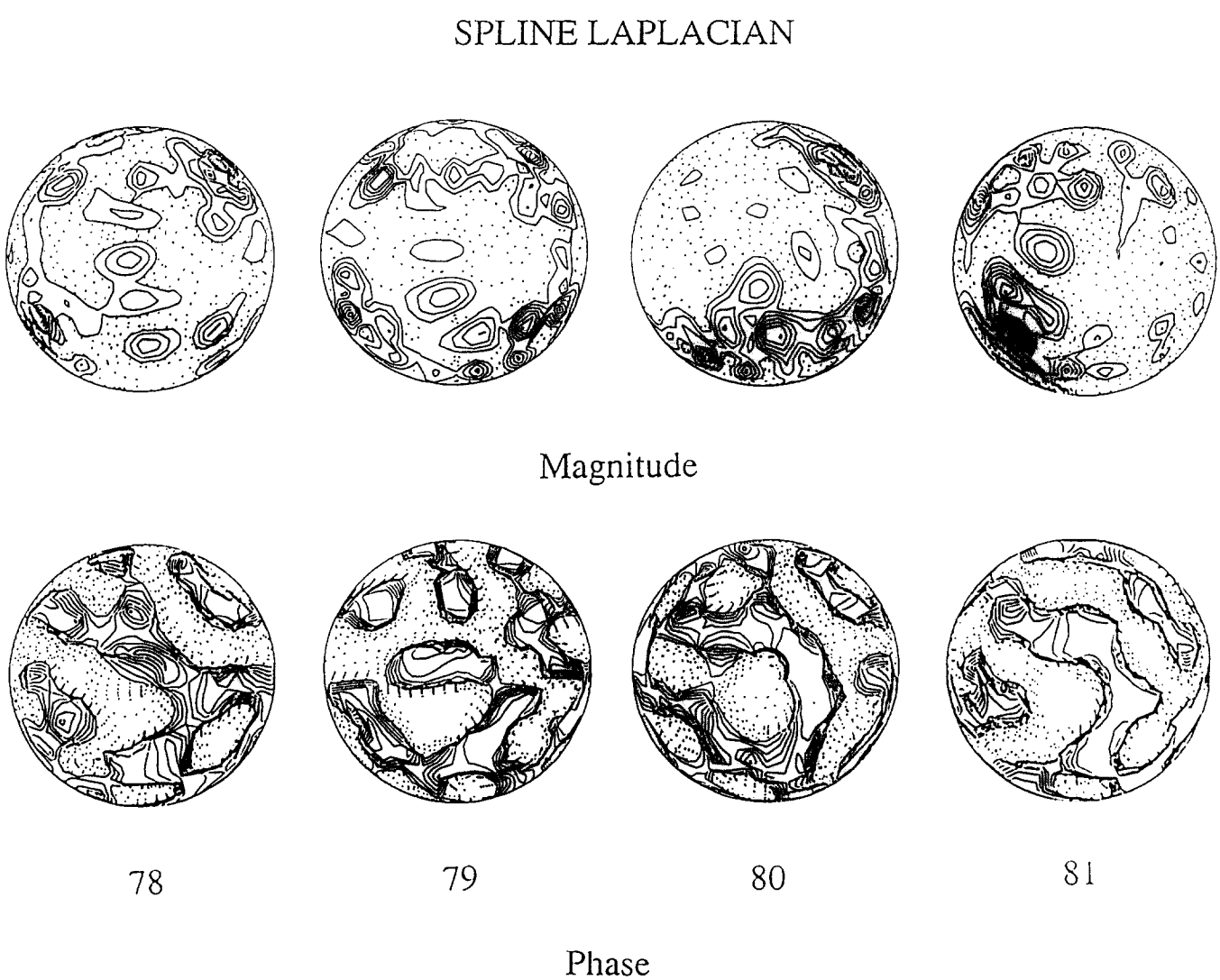

Fig. 14. Magnitude and phase plots of spline-Laplacian estimates corresponding to data shown in Fig. 13. Maximum Laplacian magnitude in the 1 Hz band is 1.5 $\mu V/cm^2$. Cosine (phase) plots have intervals of 0.15 (same as Fig. 13). The abrupt phase changes shown here occur in nearly all Laplacian and cortical image phase plots. Laplacian magnitude and phase exhibit a "quasi-stable" structure (refer to text).

aries separating regions of large phase difference (e.g., nodal lines) and boundaries separating regions of relatively large and small magnitude is also often observed.

In light of the above described data, we mention two different ideas that have been advanced to partly explain the physiological bases for alpha rhythm. One idea is that alpha rhythm originates in neocortical epicenters and spreads through the cortex as traveling waves, somewhat like raindrops in a pond (Lopes da Silva et al. 1974; Van Rotterdam et al. 1982). Another view is that alpha rhythm and other widespread EEG phenomena in humans (e.g., halothane rhythms) are partly explained as standing waves in neocortex (Nunez 1972; Nunez et al. 1977, 1981; Katznelson 1981b). The Laplacian magnitude plots appear to be consistent with the epicenter/traveling wave view, whereas the Laplacian phase plots can apparently be explained by wave interference and standing waves in a closed neocortical system. In the latter case, different spatial patterns might result from different combinations of eigenfunctions (e.g., the Y_{nm}s that form the spatial pattern), which are partly determined by on-going subcortical input (Nunez 1994). In fact, it has been suggested that these two views of EEG are not inconsistent since complex global systems are likely to produce a broad range of phenomena, including both traveling and standing waves due to both local and global mechanisms (Nunez 1989b, 1994; Nunez and Srinivasan 1993).

The future of high resolution EEG

We have demonstrated two different methods to improve the spatial resolution of scalp recorded EEG. Although the Laplacian and cortical imaging methods have different theoretical bases, they provide very similar estimates of cortical potential distribution when applied to either simulated or actual EEG data. In the case of simulated data with 64 or more spatial samples, we have shown that both methods provide accurate estimates for either isolated or distributed sources down to a scale of about 1–3 cm, depending on electrode density. We do not imply that Laplacian and cortical image estimates are equally accurate for all applications. Rather, the relatively sophisticated versions of the two approaches described here appear to be roughly equivalent, given our current state of knowledge. There are, of course, vast differences in the accuracies of different methods that have been used to estimate either Laplacians or cortical images of EEG. Thus, it is a mistake to lump all these different approaches into only two categories when accuracy issues are considered.

The simulations discussed here are based on concentric sphere models of the head. Recently, we have extended our simulations to heads with non-spherical geometry and variable skull properties using finite element models. Our preliminary experience with these simulations indicates that the high resolution methods still work very well, i.e., they provide a large improvement in accuracy over that obtained with conventional EEG.

A legitimate question is whether the mixture of theoretical and experimental studies holds up in actual EEG practice. However, this question should be addressed in the context of conventional EEG practice, which provides poor spatial resolution even in theory. Although we have not yet had the opportunity to apply our methods to EEG with known sources, we have applied the spline-Laplacian to somatosensory evoked potentials and obtained maps suggesting localized tangential dipoles at the approximate expected locations (Nunez et al. 1991). Further verification using simultaneously recorded scalp and cortical potentials is certainly called for, especially in cases of multiple cortical sources which are relatively close together. The case of multiple, close sources is generally much more challenging than that of isolated sources for high resolution methods.

As far as we know, the only study which provides a direct comparison of predicted cortical potential distribution with actual cortical potential was carried out at the EEG Systems Lab (Le and Gevins 1993). These studies involve a new finite element-based cortical imaging algorithm which includes more detailed information about head volume conductor properties than is used by the 4-sphere model. Reported predictions of cortical surface potential are quite accurate in the cases shown (isolated sources), providing further encouragement for the development of high resolution EEG.

At this stage of our understanding of high resolution EEG, a number of questions require further study:

(1) How robust is each of the methods to inaccuracies in the head model, noise in the signal, and complications of the source distribution? We have partly answered the latter two questions in this study, but much more work is required on head models.

(2) Are finite element-based cortical imaging methods significantly more accurate than spline-Laplacians or cortical imaging based on layered spheres, given that information about the head volume conductor is generally quite limited?

(3) Can we develop methods to obtain reasonably accurate electrical images of the head (Nunez 1987b)? Whereas important geometric information on tissue boundaries can be obtained from MRI and/or CT, this information may provide only a very crude idea of the electrical image. For example, preliminary in vitro measurements of skull plug resistance by the New Orleans group indicates that skull plug resistance is uncorrelated with skull thickness. A possible reason is

that skull resistance is strongly dependent on the amount of fluid that permeates the bone. Thicker skulls may have larger inner spaces so that effective resistivity decreases with thickness. The practical implication of these observations for high resolution EEG is that it is not obvious how to model skull thickness variations obtained from CT. For example, if skull resistivity were inversely proportional to thickness, local skull resistance per unit area would be constant. In this case, the main effect of skull thickness variations would be to alter distances between sources and electrodes.

Despite the open questions, we suggest that spline-Laplacian and/or cortical imaging methods based on layered spherical geometry are now ready for implementation on an experimental basis in both research and clinical settings. Whereas their exact accuracies are unknown, they provide, in theory, much better spatial resolution than conventional EEG, which does not work very well even in idealized simulations with no reference electrode complications. Thus, these new methods appear ready to supplement, if not replace, conventional EEG in a number of laboratories.

Research at Tulane University was supported by NIH Grant R01 NS243314. Research at the Swinburne Centre for Applied Neurosciences was supported by an ARC research intrastructure grant.

The authors thank Geoff Nield (in Melbourne) and Sam Law (in Seattle) for technical assistance.

References

Cadusch, P.J., Breckon, W. and Silberstein, R.B. Spherical splines and the interpolation, deblurring and transformation of topographic EEG. Pan Pacific Workshop on Brain Electric and Magnetic Topography, Melbourne, Feb. 17–18, 1992.

De Leon, M.J., George, A.E. and Ferris, S.H. Computed tomography and positron emission tomography correlates of cognitive decline in aging and senile dementia. In: L.W. Poon (Ed.), Handbook for Clinical Memory Assessment of Older Adults. American Psychological Association, New York, 1986: 367–382.

Gevins, A.S. Dynamic functional topography of cognitive tasks. Brain Topogr., 1989, 2: 37–56.

Gevins, A.S. Analysis of multiple lead data. In: J.W. Rohrbaugh, R. Parasuraman and J.R. Johnson (Eds.), Event-Related Brain Potentials. Oxford University Press, New York, 1990: 44–56.

Gevins, A.S., Brickett, P., Costales, B., Le, J. and Reutter, B. Beyond topographical mapping: towards functional-anatomical imaging with 124 channel EEG and 3-D MRIs. Brain Topogr., 1990, 3: 53–64.

Gevins, A.S., Le, J., Brickett, P., Reutter, B. and Desmond, J. Seeing through the skull: advanced EEGs accurately measure cortical activity from the scalp. Brain Topogr., 1991, 4: 125–132.

Helme, R. Private communication to R.B. Silberstein, 1991.

Hjorth, B. An on-line transformation of EEG scalp potentials into orthogonal source derivations. Electroenceph. clin. Neurophysiol., 1975, 39: 526–530.

Katznelson, R.D. In: P.L. Nunez, Electric Fields of the Brain: the Neurophysics of EEG. Oxford University Press, New York, 1981a: 197–203.

Katznelson, R.D. In: P.L. Nunez, Electric Fields of the Brain: the Neurophysics of EEG. Oxford University Press, New York, 1981b: 401–442.

Kearfott, R.B., Sidman, R.D., Major, D.J. and Hill, C.D. Numerical tests of a method for simulating electrical potentials on the cortical surface. IEEE Trans. Biomed. Eng., 1991, 38: 294–299.

Koles, Z.J. and Soong, A.C. Spatial filtering to extract abnormal and artifactual components from the electroencephalogram. In: 3rd International Congress on Brain Electromagnetic Topography, Amsterdam, June 9–12, 1992 (poster).

Lagerlund, T., Sharbrough, F. and Basacker, N. Interelectrode coherencies using nearest-neighbor and spherical harmonic expansion computation of Laplacian of scalp potential. In: 3rd International Congress on Brain Electromagnetic Topography, Amsterdam, June, 1992 (poster).

Law, S.K. Spline Generated Surface Laplacian Estimates for Improving Spatial Resolution in Electroencephalography. Ph.D. Dissertation, Tulane University, 1991.

Law, S.K., Nunez, P.L. and Wijesinghe, R.S. High resolution EEG using spline generated surface Laplacians on spherical and ellipsoidal surfaces. IEEE Trans. Biomed. Eng., 1993, 40: 145–153.

Le, J. and Gevins, A.S. Method to reduce blur distortion from EEGs using a realistic head model. IEEE Trans. Biomed. Eng., 1993, 40: 517–528.

Lopes da Silva, F.H. and Storm van Leeuwen, W. The cortical alpha rhythm in dog: the depth and surface profile of phase. In: M.A.B. Brazier and H. Petsche (Eds.), Architectonics of the Cerebral Cortex. Raven Press, New York, 1978: 319–333.

Lopes da Silva, F.H., Hoeks, H., Smiths, H. and Zetterberg, H. Model of brain rhythmic activity. Kybernetik, 1974, 15: 27–37.

Nunez, P.L. The brain wave equation: a model for the EEG. American EEG Society Meeting, Houston 1972 and Math. Biosci., 1974, 21: 279–297.

Nunez, P.L. Electric Fields of the Brain: The Neurophysics of EEG. Oxford University Press, New York, 1981.

Nunez, P.L. Locating source of the brain's electric and magnetic fields: some effects of inhomogeneity and multiple sources, with implications for the future. Human Factors and Organizational Systems Laboratory, Naval Personnel Research and Development Center, Technical Note 71-86-12. San Diego, June, 1986.

Nunez, P.L. Removal of reference electrode and volume conduction effects by spatial deconvolution of evoked potentials using a three-concentric sphere model of the head. In: The London Symposium. Electroenceph. clin. Neurophysiol., Suppl. 39. Elsevier, Amsterdam, 1987a: 143–148.

Nunez, P.L. A method to estimate local skull resistance in living subjects. IEEE Trans. Biomed. Eng., 1987b, 34: 902–904.

Nunez, P.L. Spatial filtering and experimental strategies in EEG. In: D. Samson-Dollfus (Ed.), Statistics and Topography in Quantitative EEG. Elsevier, Paris, 1988: 196–209.

Nunez, P.L. Estimation of large scale neocortical source activity with EEG surface Laplacians. Brain Topogr., 1989a, 2: 141–154.

Nunez, P.L. Generation of human EEG by a combination of long and short range neocortical interactions. Brain Topogr., 1989b, 1: 199–215.

Nunez, P.L. Physical principles and neurophysiological mechanisms underlying event-related potentials. In: J.W. Rohrbaugh, R. Parasuraman and J.R. Johnson (Eds.), Event-Related Brain Potentials. Oxford University Press, New York, 1990a: 19–36.

Nunez, P.L. Localization of brain activity with electroencephalography. In: S. Sato (Ed.), Advances in Neurology. Vol. 54. Magnetoencephalography. Raven Press, New York, 1990b: 39–65.

Nunez, P.L. Neocortical Dynamics and Human EEG Rhythms. Oxford University Press, New York, 1994: in press.

Nunez, P.L. and Pilgreen, K.L. The spline-Laplacian in clinical neurophysiology: a method to improve EEG spatial resolution. J. Clin. Neurophysiol., 1991, 8: 397–413.

Nunez, P.L. and Srinivasan, R. Implications of recording strategy for estimates of neocortical dynamics with EEG. Chaos, 1993, 3: 257–266.

Nunez, P.L., Reid, L. and Bickford, R.G. The relationship of head size to alpha frequency with implications to a brain wave model. Electroenceph. clin. Neurophysiol., 1977, 44: 344–352.

Nunez, P.L., Pilgreen, K.L., Westdorp, A.F., Law, S.K. and Nelson, A.V. A visual study of surface potentials and Laplacians due to distributed neocortical sources: computer simulations and evoked potentials. Brain Topogr., 1991, 4: 151–168.

Penfield, W. and Jasper, H. Epilepsy and the Functional Anatomy of the Human Brain. Little, Brown, Boston, MA, 1954.

Perrin, F., Bertrand, O. and Pernier, J. Scalp current density mapping: value and estimation from potential data. IEEE Trans. Biomed. Eng., 1987a, 34: 283–288.

Perrin, F., Pernier, J., Bertrand, O., Giard, M.H. and Echallier, J.F. Mapping of scalp potentials by surface spline interpolation. Electroenceph. clin. Neurophysiol., 1987b, 66: 75–81.

Perrin, F., Pernier, J., Bertrand, O. and Echallier, J.F. Spherical splines for scalp potential and current density mapping. Electroenceph. clin. Neurophysiol., 1989, 72: 184–187.

Petsche, H., Pockberger, H. and Rappelsberger, P. On the search for the sources of the electroencephalogram. Neuroscience, 1984, 11: 10–27.

Regan, D. Human Brain Electrophysiology. Evoked Potentials and Evoked Magnetic Fields in Science and Medicine. Elsevier, New York, 1989.

Shaw, G.R. Spherical Harmonic Analyses of the Electroencephalogram. Ph.D. Dissertation. University of Alberta, Edmonton, 1991.

Sidman, R.D. A method for simulating intracerebral potential fields: the cortical imaging technique. J. Clin. Neurophysiol., 1991, 8: 432–441.

Silberstein, R.B. and Cadusch, P.J. Measurement processes and spatial principal component analysis. Brain Topogr., 1992, 4: 267–276.

Silberstein, R.B., Ciorciari, J., Pipingas, A., Schier, M.A. and Ma, S. Effects of the Wisconsin card sort test on the topography of the steady state visually evoked potential. In: 3rd International Congress on Brain Electromagnetic Topography, Amsterdam, June 9–12, 1992.

Stephenson, W.A. and Gibb, W.A. A balanced non-cephalic reference electrode. Electroenceph. clin. Neurophysiol., 1951, 3: 237–240.

Van Rotterdam, A., Lopes da Silva, F.H., Van der Ende, J., Viergever, M.A. and Hermans, A.J. A model of the spatial-temporal characteristics of the alpha rhythm. Bull. Math. Biol., 1982, 44: 283–305.

Wahaba, G. Spline interpolation and smoothing on a sphere. Siam J. Sci. Stat. Comput., 1981, 2: 5–16.

Yan, Y., Nunez, P.L. and Hart, R.T. A finite element model of the human head: scalp potentials due to dipole sources. Med. Biol. Eng. Comput. 1991, 29: 475–481.